

Analysis of 70 Ophiuchi AB including seismic constraints

P. Eggenberger¹, A. Miglio¹, F. Carrier², J. Fernandes³, and N.C. Santos⁴

¹ Institut d'Astrophysique et de Géophysique de l'Université de Liège, 17 Allée du 6 Août, B-4000 Liège, Belgium
e-mail: eggenberger@astro.ulg.ac.be; miglio@astro.ulg.ac.be

² Institute of Astronomy, University of Leuven, Celestijnenlaan 200 B, B-3001 Leuven, Belgium
e-mail: fabien@ster.kuleuven.be

³ Observatório Astronómico da Universidade de Coimbra e Departamento de Matemática, FCTUC, Portugal
e-mail: jmfernan@mat.uc.pt

⁴ Centro de Astrofísica, Universidade do Porto, Rua das Estrelas, P-4150-762 Porto, Portugal
e-mail: nuno@astro.up.pt

Received; accepted

ABSTRACT

Context. The analysis of solar-like oscillations for stars belonging to a binary system provides a unique opportunity to probe the internal stellar structure and to test our knowledge of stellar physics. Such oscillations have been recently observed and characterized for the A component of the 70 Ophiuchi system.

Aims. We determined the global parameters of 70 Ophiuchi AB using the new asteroseismic measurements now available for 70 Oph A and tested the input physics introduced in stellar evolution codes.

Methods. Three different stellar evolution codes and two different calibration methods were used to perform a comprehensive analysis of the 70 Ophiuchi system.

Results. A model of 70 Ophiuchi AB that correctly reproduces all observational constraints available for both stars is determined. An age of 6.2 ± 1.0 Gyr is found with an initial helium mass fraction $Y_i = 0.266 \pm 0.015$ and an initial metallicity $(Z/X)_i = 0.0300 \pm 0.0025$ when atomic diffusion is included and a solar value of the mixing-length parameter assumed. A precise and independent determination of the value of the mixing-length parameter needed to model 70 Oph A requires accurate measurement of the mean small separation, which is not available yet. Current asteroseismic observations, however, suggest that the value of the mixing-length parameter of 70 Oph A is lower or equal to the solar calibrated value. The effects of atomic diffusion and of the choice of the adopted solar mixture were also studied. We finally found that the different evolution codes and calibration methods we used led to perfectly coherent results.

Key words. stars: oscillations – stars: interiors – stars: fundamental parameters – stars: binaries: visual – stars: individual: 70 Ophiuchi

1. Introduction

The solar five-minute oscillations have provided a wealth of information on the internal structure of the Sun. These results stimulated various attempts to detect a similar signal on other solar-type stars by photometric or equivalent width measurements. In past years, the stabilized spectrographs developed for extra-solar planet search have finally achieved the accuracy needed to detect solar-like oscillations on other stars (see e.g. Bedding & Kjeldsen 2007). A major difficulty is the confrontation between these observations and theoretical models. The classical observational measurements available for an isolated star (effective temperature, metallicity, luminosity) combined with the oscillation frequencies provide strong constraints to the global parameters of the star but are often not sufficient to unambiguously determine a unique model and to really test the input physics included in the computation of the stellar models (see for example the case of the isolated star β Virginis, Eggenberger & Carrier 2006). In this regard, binary stars constitute ideal asteroseismic targets in order to test our knowledge of stellar physics. In the case of a binary system, we can indeed assume that both stars share the same age and initial chemical composition. The additional constraints imposed by this assumption are then extremely valuable to accurately determine the global

properties of the stars. Moreover, in the case of a binary system, the masses of both components are accurately known by combining visual and spectroscopic orbits.

Unfortunately, individual frequencies of solar-like oscillations have only been identified for stars belonging to two different binary systems: the G2 dwarf star α Cen A (Bouchy & Carrier 2002; Bedding et al. 2004; Bazot et al. 2007), the K1 dwarf star α Cen B (Carrier & Bourban 2003; Kjeldsen et al. 2005) and the F5 IV-V star Procyon A (Martić et al. 2004; Eggenberger et al. 2004a; Mosser et al. 2007). Recently, Carrier & Eggenberger (2006) reported the detection of solar-like oscillations on the bright K0 dwarf star 70 Ophiuchi A (HD 165341A) belonging to the nearby visual binary system 70 Ophiuchi, which is among the first discovered binary systems. The aim of the present paper is to perform a comprehensive calibration of the 70 Ophiuchi system that includes the new seismological data available for the A component. In addition to the determination of the 70 Ophiuchi AB global parameters, we also test and compare the theoretical tools used for the modeling of stars for which p-modes frequencies are detected by performing this analysis with three different stellar evolution codes and two different calibration methods. This work therefore takes place in the continuity of the work undertaken by the Evolution and Seismic Tools Activity (ESTA) group within the CoRoT mission (Monteiro et al. 2006).

Table 1. Orbital elements derived for the 70 Ophiuchi system when all available measurements (speckle and radial velocity) are included (see text for more details).

Parameter	Value
P (days)	32279 ± 15
T_0 (HJD)	45809 ± 14
e	0.5005 ± 0.0006
V_0 (km s^{-1})	-7.026 ± 0.015
i	121.1 ± 0.1
ω (deg)	193.4 ± 0.3
Ω (deg)	121.7 ± 0.2
K_1 (km s^{-1})	3.51 ± 0.04
K_2 (km s^{-1})	4.25 ± 0.05
a (arcsec)	4.526 ± 0.007
M_1 (M_\odot)	0.89 ± 0.02
M_2 (M_\odot)	0.73 ± 0.01
π (mas)	194.2 ± 1.2

The observational constraints available for the 70 Ophiuchi system are summarized in Sect. 2. The input physics and the computational methods used for the calibrations are described in Sect. 3. The results are presented in Sect. 4, while the conclusion is given in Sect. 5.

2. Observational constraints

2.1. Binarity

70 Ophiuchi is a very well studied stellar system composed of a K0 and K5 dwarf star with an orbital period of 88.38 yr (Pourbaix 2000). It is known as a binary by both spectroscopy and speckle interferometry. Radial-velocity curves were first obtained by Batten et al. (1984) and Batten & Fletcher (1991), while the whole orbit (speckle and radial velocity) was published by Pourbaix (2000). This binary system was observed over 6 nights in July 2004 with the HARPS spectrograph mounted on the 3.6-m telescope at La Silla Observatory (ESO, Chile) (Carrier & Eggenberger 2006). Combining our new radial-velocity measurements with previous ones (Pourbaix et al. 2004), we use the ORBIT code made available by T. Forveille and developed in Grenoble (Forveille et al. 1999) to simultaneously fit the radial velocities and the speckle measurements (see Fig. 1 and 2). Note that the very high precision of the new HARPS data is quite important in order to derive an accurate value for K_2 and hence a reliable mass for the B component. Moreover, these new data add an important observation of the radial velocity of 70 Oph B since only few measurements were previously obtained for this component (see Fig. 1). The values of the derived orbital parameters, of the parallax, and of the masses of both components are listed in Table 1. We note that the value of the parallax derived in this way (194.2 ± 1.2 mas) is in good agreement with the value of 195.7 ± 0.9 mas determined by Söderhjelm (1999) using the Hipparcos astrometry with ground-based observations available at that time.

2.2. Effective temperatures and chemical composition

The effective temperature and iron abundance of the two stars were obtained from our own HARPS spectra by following the methodology and line-lists used in Santos et al. (2004). This determination makes use of an iterative procedure based on

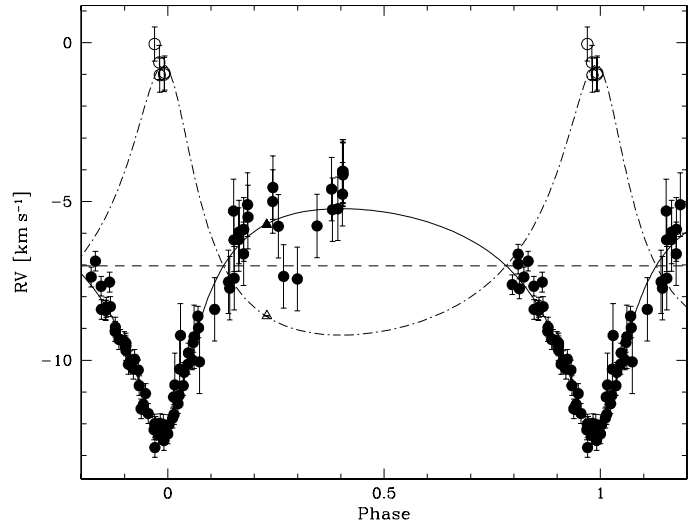


Fig. 1. Radial velocity orbit of the 70 Ophiuchi system. Full and open symbols correspond to 70 Oph A and B, respectively. Triangles indicate the new HARPS measurements, while circles indicate previous measurements.

iron excitation and ionization equilibrium. We refer to this paper for more details. The results of this method were shown to give excellent results for solar-type stars, and the derived stellar parameters, namely the effective temperature, are compatible with those derived from other methods (e.g. the IR-flux method, Casagrande et al. 2006). For the metallicity of the system a mean value of $[\text{Fe}/\text{H}] = 0.04 \pm 0.05$ was thus determined and used for the present calibration. No α -element enhancement is suggested for the 70 Ophiuchi system by current spectroscopic data. Concerning the effective temperature, we derived a value of 5300 ± 50 K for the A component. For the B component, an effective temperature of 4205 K is found with an uncertainty estimated to 100 K. We however note that our spectroscopic determination is less adapted for this kind of cold star. We thus decided to adopt as $T_{\text{eff}}^{\text{B}}$ a mean value between our determined spectroscopic temperature of 4205 K, our photometric deduced value of 4220 K (see Section 2.3) and the effective temperature of 4740 K determined by Luck & Heiter (2005). In this way a mean temperature of $T_{\text{eff}}^{\text{B}} = 4390$ K was determined for the B component. We also decided to adopt a large error of 200 K on the effective temperature of 70 Oph B, so that our calibration of the system is only weakly constrained by this value, which is not precisely determined.

2.3. Luminosities

From 1977 to 2005, the 70 Ophiuchi system has been measured in the GENEVA photometric system (Golay 1980) with the photoelectric photometer P7 (Burnet & Rufener 1979) installed first on the Swiss telescope in La Silla (ESO, Chile) and then on the Belgian telescope at La Palma. Nine measurements were obtained. However, due to the small separation between components and to too large a diaphragm, these photometric measurements only represent the mean flux of both components $V_{\text{tot}} = 4.012 \pm 0.013$, $V_{1\text{tot}} = 4.779 \pm 0.013$ and $B_{2\text{tot}} = 5.323 \pm 0.015$ mag. In order to obtain individual photometric measurements of both components, the 70 Ophiuchi system was observed with the CCD camera C2 installed on the Swiss telescope at La Silla (Cherix et al. 2006) between 2005 August 20-23 using very short exposure times of 0.02,

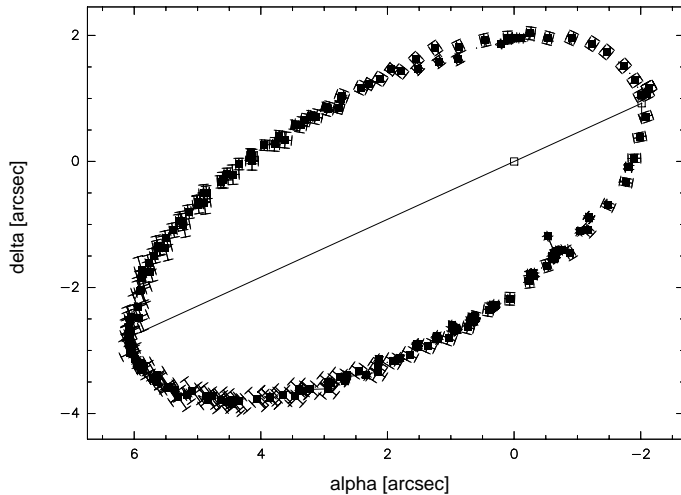


Fig. 2. Apparent visual orbit of the 70 Ophiuchi system. The solid line indicates the line of nodes, while the square indicates the position of the periastron.

Table 2. Observational constraints for 70 Oph A and B.

	70 Oph A	70 Oph B
π (mas)	194.2 ± 1.2	
M/M_{\odot}	0.89 ± 0.02	0.73 ± 0.01
V (mag)	4.191 ± 0.014	6.061 ± 0.021
L/L_{\odot}	0.53 ± 0.02	0.15 ± 0.02
T_{eff} (K)	5300 ± 50	4390 ± 200
[Fe/H]	0.04 ± 0.05	
$\Delta\nu_0$ (μHz)	161.8 ± 0.8	-

0.03 and 0.2 s in the V , $V1$ and $B2$ bands, respectively. A large number of exposures were obtained in order to reduce the noise due in great part to the scintillation: 80, 18 and 12 exposures were thus taken in the V , $V1$ and $B2$ filters, respectively. These CCD frames allowed us to determine the luminosity shifts between both components; we thus found a difference of 1.870 ± 0.014 , 1.920 ± 0.014 and 2.255 ± 0.028 mag in the V , $V1$ and $B2$ bands, respectively. Combining these values with the previous ones, we finally derived mean visual magnitudes $V_A = 4.191 \pm 0.014$ and $V_B = 6.061 \pm 0.021$ mag and photometric indexes $(B2 - V1)_A = 0.501 \pm 0.020$ and $(B2 - V1)_B = 0.836 \pm 0.040$ for the 70 Ophiuchi system. Note that these indexes lead to an effective temperature of 4220 K for the B component (Ramírez & Meléndez 2005).

Combining the mean magnitudes with the parallax deduced from the radial-velocity and speckle orbits ($\pi = 194.2 \pm 1.2$), and by using the solar absolute bolometric magnitude $M_{\text{bol},\odot} = 4.746$ (Lejeune et al. 1998) with the bolometric corrections from Flower (1996) ($BC_A = -0.20 \pm 0.02$ and $BC_B = -0.69 \pm 0.17$ mag), the luminosities are finally determined with a value of $0.53 \pm 0.02 L_{\odot}$ for 70 Oph A and $0.15 \pm 0.02 L_{\odot}$ for 70 Oph B.

2.4. Asteroseismic constraints

Solar-like oscillations in 70 Ophiuchi A were recently observed by Carrier & Eggenberger (2006) with the HARPS echelle spectrograph. Fourteen oscillation frequencies were detected in the power spectrum between 3 and 6 mHz with amplitudes in the

range 11 to 14 cm s^{-1} . Unfortunately, the mono-site nature of the observations, coupled to the low resolution of the time series and to the faint signal-to-noise, do not allow a unique identification of the detected frequencies. Indeed, the small separation between $\ell = 2$ and $\ell = 0$ modes is not clearly detected and the $\ell = 2$ modes cannot therefore be unambiguously disentangled from the $\ell = 0$ modes. Consequently $\ell = 0, 2$ can be replaced by $\ell = 1$ modes and $\ell = 1$ by $\ell = 2$ modes. Although these measurements cannot allow an unambiguous identification of individual detected oscillation frequencies, they provide us with a precise determination of the mean large separation of 70 Oph A. By averaging the 4 different large separations observed for the modes listed as $\ell = 0$ modes in Table 3 of Carrier & Eggenberger (2006) with an uncertainty on individual frequencies estimated to half the time resolution, we obtain a mean value $\Delta\nu_0 = 161.8 \pm 0.8 \mu\text{Hz}$ that is used in the present computations. We note that the error on this value is slightly larger than the uncertainty of $0.3 \mu\text{Hz}$ quoted by Carrier & Eggenberger (2006) who included large separation averages taken between non-consecutive modes.

Although the mean small separation of 70 Oph A cannot be clearly determined from current asteroseismic measurements, these observations nevertheless suggest that this value must be included in a frequency interval centered around the daily alias of $11.57 \mu\text{Hz}$ introduced by the mono-site observations and delimited by the frequency resolution of the time-series ($2.2 \mu\text{Hz}$). Indeed, if the value of the small separation of 70 Oph A differs from $11.57 \pm 2.2 \mu\text{Hz}$, we can then reasonably think that it should have been revealed by existing asteroseismic measurements. The inclusion of this additional observational constraint in the calibration of the 70 Ophiuchi system is discussed in detail in Sect. 4.1.

3. Stellar models

3.1. Input Physics

Three different stellar evolution codes are used for these computations: the Geneva code (Meynet & Maeder 2000; Eggenberger et al. 2007), the CLES code (Code Liégeois d'Evolution Stellaire, Scuflaire et al. 2007b) and the CESAM code (Code d'Evolution Stellaire Adaptatif et Modulaire, Morel 1997).

These three stellar evolution codes are described in detail in the above mentioned references. We simply note that the Geneva code uses the MHD equation of state (Hummer & Mihalas 1988; Mihalas et al. 1988; Däppen et al. 1988) and the NACRE nuclear reaction rates (Angulo et al. 1999). The CLES code uses the OPAL equation of state (Rogers & Nayfonov 2002) in its 2005 version and the NACRE nuclear reaction rates, while the version of the CESAM code used for the present computations includes the EFF equation of state (Eggleton et al. 1973) and the nuclear reaction rates given by Caughlan & Fowler (1988). All codes use the opacity tables from the OPAL group (Iglesias & Rogers 1996) complemented at low temperatures with Alexander & Ferguson (1994) opacities and the standard mixing-length formalism for convection. The diffusion due to the concentration and thermal gradients is also included in the computations, but the radiative acceleration is neglected as it is negligible for the structure of low-mass stellar models with extended convective envelopes (Turcotte et al. 1998).

A solar calibration has first been performed with the three evolution codes. A mixing-length parameter $\alpha = 1.7998$ and an initial helium mass fraction $Y_1 = 0.2735$ is then determined with the physics included in the Geneva code. The input physics

used by the CLES code leads to $\alpha = 1.8544$ and $Y_i = 0.2755$, while values of $\alpha = 1.7985$ and $Y_i = 0.2848$ are found with the CESAM code. We note that the higher value of the solar calibrated mixing-length parameter found for the CLES code mainly results from the use of Kurucz (1998) atmosphere models in the CLES code instead of the grey atmosphere approximation included in the other evolution codes. Likewise, the CESAM code gives a higher value of the solar calibrated initial helium mass fraction, which is mainly due to the use of the EFF equation of state instead of the OPAL and MHD equations of state introduced in the CLES and Geneva codes.

3.2. Calibration methods

Basically, the calibration of a binary system consists in finding the set of stellar modeling parameters that best reproduces all observational data available for both stars. The characteristics of a stellar model depend on five modeling parameters: the mass M of the star, its age (hereafter t), the mixing-length parameter $\alpha \equiv l/H_p$ for convection and two parameters describing the initial chemical composition of the star. For these two parameters, we choose the initial helium abundance Y_i and the initial ratio between the mass fraction of heavy elements and hydrogen $(Z/X)_i$. This ratio is directly related to the abundance ratio $[\text{Fe}/\text{H}]$ assuming that $\log(Z/X) \cong [\text{Fe}/\text{H}] + \log(Z/X)_\odot$. In this study, stellar models are computed with the solar value $(Z/X)_\odot = 0.0245$ given by Grevesse & Noels (1993) as well as with the new solar mixture of Asplund et al. (2005) complemented with the neon abundance of Cunha et al. (2006), which results in a lower value $(Z/X)_\odot = 0.0178$.

The binary nature of the system leads to a precise determination of the mass of both components. By assuming that both components of a binary system share the same age and initial chemical composition, three additional constraints are obtained: $t_A = t_B$, $Y_i^A = Y_i^B$ and $(Z/X)_i^A = (Z/X)_i^B$. Consequently, we have to determine a set of seven modeling parameters (t , M_A , M_B , α_A , α_B , Y_i and $(Z/X)_i$). In the case of 70 Ophiuchi, we also assume that the value of the mixing-length parameter is identical for both components of the system ($\alpha_A = \alpha_B$). This assumption results from the limited number of observational constraints available for the B component of the system. Indeed, no asteroseismic measurements are available for 70 Oph B and its effective temperature is only determined with a large error of 200 K (see Table 2).

Following the work done for the analysis of the α Centauri system, the determination of the set of modeling parameters (t , M_A , M_B , α , Y_i and $(Z/X)_i$) leading to the best agreement with the observational constraints is made by using two different calibration methods. The first one is based on the computation of a dense grid of stellar models as explained in Eggenberger et al. (2004b), while the second one uses the gradient-expansion algorithm known as Levenberg-Marquardt method (see Miglio & Montalbán 2005). The reader is referred to these two references for a detailed description of the methods. In the present study, the grid of stellar models was computed by varying the masses of 70 Ophiuchi A and B within their observational errors by step of $0.01 M_\odot$. Concerning the chemical composition, the initial helium abundance Y_i was changed between 0.240 and 0.290 by step of 0.002. Models of 70 Oph B computed with an initial helium mass fraction larger than 0.290 are indeed found to be too luminous to correctly reproduce the observed luminosity. For the initial value of the ratio between the mass fraction of heavy elements and hydrogen $(Z/X)_i$, we first note that the surface metallicities $[\text{Fe}/\text{H}]_s$ are almost iden-

tical for models of 70 Ophiuchi with the same initial composition and different mixing-length parameters α . Moreover, the $[\text{Fe}/\text{H}]_s$ of the models are mainly sensitive to $(Z/X)_i$ and less to Y_i . As a result, the values of $(Z/X)_i$ are directly constrained by the observed surface metallicities; we found that the models matching the observed metallicities have $(Z/X)_i$ ranging from about 0.027 to 0.033 (i.e. an initial metallicity $[\text{Fe}/\text{H}]_i$ between 0.04 and 0.13). The value of the mixing-length parameter was changed between 0.8 and $1.3\alpha_\odot$ with a typical step of $0.02\alpha_\odot$. Finally, we note that the age of the models was limited to 15 Gyr and that a model of 70 Oph A is considered to have the same age as a model of 70 Oph B when the difference is lower than 0.01 Gyr.

The theoretical low- ℓ p-mode frequencies of 70 Oph A are calculated using the Aarhus adiabatic pulsation package (Christensen-Dalsgaard 1997) for models computed with the Geneva and the CESAM code, while the Liège oscillation code (Scuflaire et al. 2007a) is used for models computed with the CLES code. The value of the mean large separation is determined for each model of 70 Oph A by making the average of the theoretical separations corresponding to the observed frequencies (see Sect. 2.4). A χ^2 minimization is then performed by defining the following functional that includes the observational constraints (classical as well as asteroseismic) currently available for both components of 70 Ophiuchi

$$\chi^2 \equiv \sum_{i=1}^{N_{\text{tot}}} \left(\frac{C_i^{\text{theo}} - C_i^{\text{obs}}}{E_i^{\text{obs}}} \right)^2, \quad (1)$$

where N_{tot} is the total number of observational constraints included in the calibration. The vectors \mathbf{C} contains therefore all observables for both stars:

$$\mathbf{C} \equiv (M_A, M_B, L_A, L_B, T_{\text{eff}}^A, T_{\text{eff}}^B, [\text{Fe}/\text{H}]_s^A, [\text{Fe}/\text{H}]_s^B, \Delta\nu_0^A).$$

The vector \mathbf{C}^{theo} contains the theoretical values of these observables for the model to be tested, while the values of \mathbf{C}^{obs} are those listed in Table 2. The vector \mathbf{E}^{obs} contains the errors on these observations, which are also given in Table 2.

4. Results

Using the observational constraints listed in Sect. 2, we perform the aforementioned χ^2 minimization. In a first time, we fix the mixing-length parameter to its solar calibrated value: $\alpha_A = \alpha_B = \alpha_\odot$. The solar mixture of Grevesse & Noels (1993) is used and atomic diffusion of helium and heavy elements is included in the computation.

The calibration is first performed by computing a dense grid of stellar models with the Geneva stellar evolution code. In this way, we find the following solution $t = 6.2 \pm 1.0$ Gyr, $M_A = 0.91 \pm 0.02 M_\odot$, $M_B = 0.72 \pm 0.01 M_\odot$, $Y_i = 0.266 \pm 0.015$ and $(Z/X)_i = 0.0300 \pm 0.0025$. The position in the HR diagram of this model of 70 Oph A and B (denoted model M1a in the following) is given in Fig. 3. The characteristics of this model are reported in Table 3. The confidence limits of each modeling parameter given in Table 3 are estimated as the maximum/minimum values that fit the observational constraints when the other calibration parameters are fixed to their medium value.

In order to compare results obtained by using a different stellar evolution code, the same calibration is done by using the CLES code and the Levenberg-Marquardt method. This calibration (called model M1b) leads to the following solution: $t = 6.5 \pm 1.0$ Gyr, $M_A = 0.90 \pm 0.02 M_\odot$, $M_B = 0.73 \pm 0.01 M_\odot$,

Table 3. Models for 70 Oph A and B obtained with three different stellar evolution codes. The M1 models are computed with the solar mixture of Grevesse & Noels (1993) and include atomic diffusion of helium and heavy elements. Model M2 is computed with the new solar mixture of Asplund et al. (2005) complemented with the neon abundance of Cunha et al. (2006) and includes atomic diffusion of helium and heavy elements. Model M3 is computed with the solar mixture of Grevesse & Noels (1993) but without atomic diffusion. These models are computed with a solar-calibrated value of the mixing-length parameter. The upper part of the table gives the non-asteroseismic observational constraints used for the calibration. The middle part of the table gives the modeling parameters with their confidence limits, while the bottom part presents the global parameters of both stars.

	Model M1a Geneva code		Model M1b CLEs code		Model M1c CESAM code		Model M2 Solar mixture: Asp+Cunha		Model M3 No atomic diffusion	
	70 Oph A	70 Oph B	70 Oph A	70 Oph B	70 Oph A	70 Oph B	70 Oph A	70 Oph B	70 Oph A	70 Oph B
M/M_{\odot}	0.89 ± 0.02	0.73 ± 0.01	0.89 ± 0.02	0.73 ± 0.01	0.89 ± 0.02	0.73 ± 0.01	0.89 ± 0.02	0.73 ± 0.01	0.89 ± 0.02	0.73 ± 0.01
L/L_{\odot}	0.53 ± 0.02	0.15 ± 0.02	0.53 ± 0.02	0.15 ± 0.02	0.53 ± 0.02	0.15 ± 0.02	0.53 ± 0.02	0.15 ± 0.02	0.53 ± 0.02	0.15 ± 0.02
T_{eff} (K)	5300 ± 50	4390 ± 200	5300 ± 50	4390 ± 200	5300 ± 50	4390 ± 200	5300 ± 50	4390 ± 200	5300 ± 50	4390 ± 200
[Fe/H]	0.04 ± 0.05		0.04 ± 0.05		0.04 ± 0.05		0.04 ± 0.05		0.04 ± 0.05	
M/M_{\odot}	0.91 ± 0.02	0.72 ± 0.01	0.90 ± 0.02	0.73 ± 0.01	0.91 ± 0.02	0.72 ± 0.01	0.90 ± 0.02	0.73 ± 0.01	0.90 ± 0.02	0.73 ± 0.01
t (Gyr)	6.2 ± 1.0		6.5 ± 1.0		6.2 ± 1.0		6.3 ± 1.0		7.2 ± 1.2	
Y_i	0.266 ± 0.015		0.266 ± 0.018		0.272 ± 0.015		0.255 ± 0.018		0.254 ± 0.018	
$(Z/X)_i$	0.0300 ± 0.0025		0.0300 ± 0.0025		0.0300 ± 0.0025		0.0220 ± 0.0023		0.0266 ± 0.0025	
L/L_{\odot}	0.527	0.152	0.521	0.163	0.535	0.152	0.522	0.164	0.522	0.163
T_{eff} (K)	5293	4438	5283	4434	5290	4395	5284	4445	5286	4437
R/R_{\odot}	0.865	0.661	0.863	0.685	0.872	0.674	0.864	0.684	0.863	0.684
Y_s	0.238	0.248	0.238	0.247	0.244	0.253	0.228	0.237	0.254	0.254
$(Z/X)_s$	0.0269	0.0280	0.0267	0.0279	0.0266	0.0277	0.0192	0.0201	0.0266	0.0266
[Fe/H] _s	0.04	0.06	0.04	0.06	0.04	0.05	0.04	0.06	0.04	0.04

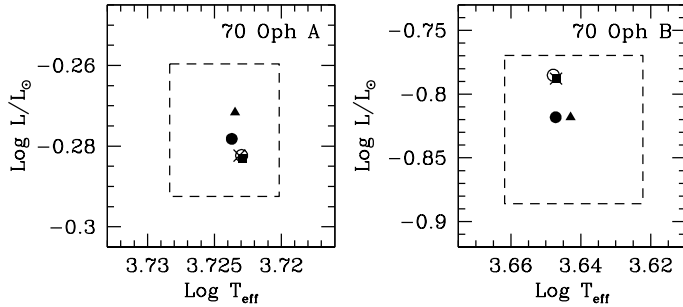


Fig. 3. Location in the HR diagram for the models of 70 Oph A and B. The dashed lines indicate the boxes delimited by the observed luminosities and effective temperatures (with their respective 1-sigma errors). The dot, the square and the triangle correspond to the M1a, M1b and M1c models, respectively. The open circle indicates the position of the M2 model, while the cross corresponds to the M3 model. Note that the symbols corresponding to the M1b, M2 and M3 models are partly superimposed. In particular, the crosses corresponding to the M3 model are superimposed to the squares indicating the location of the M1b model.

$Y_i = 0.266 \pm 0.018$ and $(Z/X)_i = 0.0300 \pm 0.0025$. The characteristics of this solution are given in Table 3 and the location of both components in the HR diagram is shown in Fig. 3. A third comparison is finally performed by using the CESAM evolution code. The following solution (denoted model M1c) is then found: $t = 6.2 \pm 1.0$ Gyr, $M_A = 0.91 \pm 0.02 M_{\odot}$, $M_B = 0.72 \pm 0.01 M_{\odot}$, $Y_i = 0.272 \pm 0.015$ and $(Z/X)_i = 0.0300 \pm 0.0025$. The global parameters of 70 Oph AB determined with this solution are also given in the bottom part of Table 3, while Fig. 3 shows the location of both components in the HR diagram.

From these results, we first conclude that a consistent model of the 70 Ophiuchi system that correctly reproduces all observational constraints now available for 70 Oph A and B can be determined. Indeed, Fig. 3 and Table 3 show that the three solutions are in very good agreement with all classical observables included in the calibration. Moreover, the M1 models correctly reproduce the observed value of the mean large separation of

70 Oph A. Note that the global asteroseismic features of the three M1 models of 70 Oph A are very similar; they all exhibit a mean large separation of about $161.8 \mu\text{Hz}$ with a mean small separation between $\ell = 2$ and $\ell = 0$ of about $9.5 \mu\text{Hz}$. As an illustration, the variation in the large and small separation $\delta\nu_{02}$ with frequency for the M1b model of 70 Oph A is shown in Fig. 4. From Table 3 we also conclude that the three different stellar evolution codes give very similar results. We only note a slightly higher value of the initial helium mass fraction determined with the CESAM evolution code, which is directly related to the higher value of this parameter found for the solar calibration (see Sect. 3.1). These results are comforting since the input physics included in these three codes is similar (although not strictly identical, see Sect. 3.1) and must therefore lead to a coherent determination of the modeling parameters of the 70 Ophiuchi system. It is also worthwhile to recall here that, in addition to the stellar evolution codes, the calibration methods were compared. Indeed, the M1a model has been obtained by computing a dense grid of stellar models, while the solution M1b has been determined by using an optimization algorithm. We thus find that these methods lead to the same determination of the global parameters of 70 Oph AB. These results are in good agreement with previous computations done for the calibration of the α Centauri system by using the Geneva and the CLES evolution code (see Eggenberger et al. 2004b; Miglio & Montalbán 2005). We also note that the values of the parameters that we found for the 70 Ophiuchi system are globally in good agreement with the results of previous studies by Fernandes et al. (1998) and Casagrande et al. (2007) with smaller error bars resulting from the numerous observational constraints now available for this system.

Thus an age of about 6 Gyr with a typical uncertainty of 1 Gyr is determined for the 70 Ophiuchi system independently of the evolution code used for the computation. Concerning the initial chemical composition, we find an initial ratio between the mass fraction of heavy elements and hydrogen $(Z/X)_i = 0.0300 \pm 0.0025$, which is slightly higher than for a solar model. This value is directly constrained by the observed surface metallicity $[\text{Fe}/\text{H}]_s = 0.04 \pm 0.05$. Contrary to the initial ratio between the mass fraction of heavy elements and hydrogen, a

slightly lower value of the initial helium abundance is found for 70 Oph AB than for a solar model. We however note that the error on this parameter is large. Moreover, we recall here that all these results have been obtained by fixing the mixing-length parameter of both components of the 70 Ophiuchi system to the solar calibrated value. We are now interested in investigating which solutions can be found by relaxing this constraint.

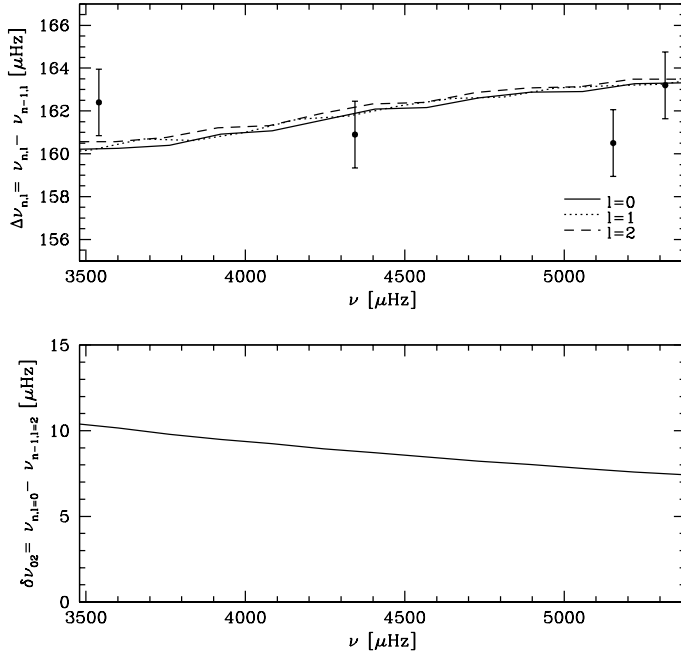


Fig. 4. Large and small separations versus frequency for the M1b model of 70 Oph A. The dots indicate the observed values of the large separation with an uncertainty on individual frequencies estimated to half the time resolution ($1.1 \mu\text{Hz}$).

4.1. Models with a free mixing-length parameter

The calibration of the 70 Ophiuchi system is then done by relaxing the constraint of a solar mixing-length parameter. We however still assume that the mixing-length parameter of 70 Oph A is equal to the one of the B component. We then find that models with different values of the initial helium abundance are able to correctly reproduce all observational constraints now available for the 70 Ophiuchi system. This is due to the fact that a decrease (increase) of the initial helium abundance Y_i can be compensated by an increase (decrease) of the mixing-length parameter α to match the observed position of 70 Oph A in the HR diagram as found previously for the calibration of the star Procyon A (see Eggenberger et al. 2005). As an illustration, Fig. 5 shows the evolutionary track of 70 Oph A for a model computed with an initial helium abundance $Y_i = 0.240$ and a mixing-length parameter $\alpha = 1.25\alpha_\odot$. This model shares approximately the same location in the HR diagram as the M1a model but exhibits a much higher age of about 10.5 Gyr due to its very low initial helium abundance. We thus obtain a series of models with approximately the same non-asteroseismic features as those of the M1 models computed with a solar calibrated value of the mixing-length parameter. Moreover, the mean large separation of these models (which is the only asteroseismic quantity included in the χ^2 functional) is also very close to the value of the M1a model,

since it mainly depends on the square root of the star’s mean density.

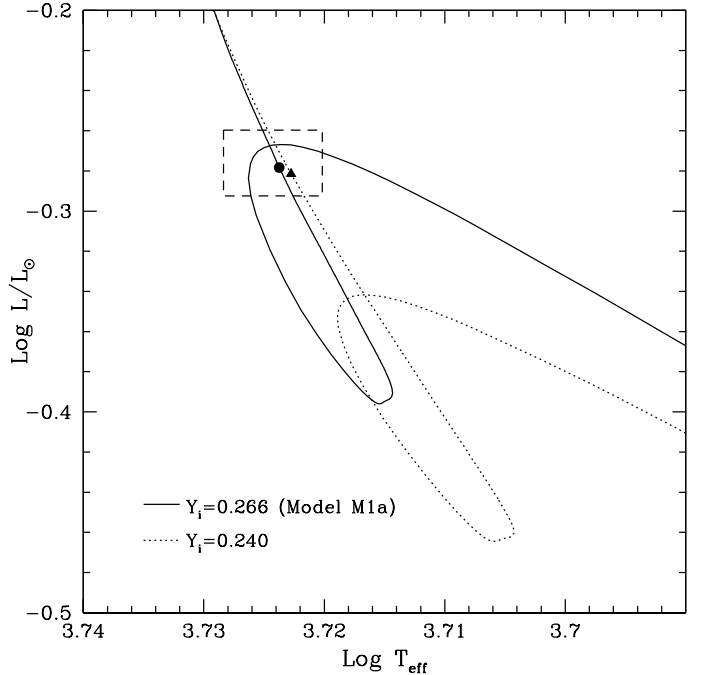


Fig. 5. Evolutionary tracks in the HR diagram for two models of 70 Oph A with different values of the initial helium mass fraction Y_i and convection parameter α . The model M1a computed with $Y_i = 0.266$ has a solar mixing-length parameter, while the solution with a lower initial helium mass fraction of $Y_i = 0.240$ exhibits a higher value of this parameter ($\alpha = 1.25\alpha_\odot$). This shows that a decrease in the initial helium mass fraction can be compensated by an increase of the mixing-length parameter in order to reach the same location in the HR diagram.

The observed location of 70 Oph B in the HR diagram only provides weak constraints to discriminate between these models because of the large error on its effective temperature and because the model of 70 Oph B spend most of its time within the observational box in the HR diagram during its main-sequence evolution due to its low mass of $0.73 M_\odot$. Only solutions with an initial helium abundance Y_i larger than about 0.290 (corresponding to an age lower than about 2 Gyr) lead to models of 70 Oph B with a too high luminosity to reproduce the classical observations. This explains why there is a series of models of 70 Oph AB with very different ages and initial helium abundances that well reproduce the global stellar parameters considered in the calibration. We however note that these models exhibit different asteroseismic features although they are characterized by the same value of the mean large separation. In particular, these models have different values of the mean small separation $\delta\nu_{02}$ since their ages differ. This is shown in Fig. 6 where the large and small separations of 70 Oph A for the M1a model and for the model computed with $Y_i = 0.240$ are compared. We see that both models are characterized by the same values of the large separations, while the mean small separation $\delta\nu_{02}$ of the M1a model is significantly larger ($3 \mu\text{Hz}$) than the one of the model with a lower initial helium abundance. This illustrates the importance of having a precise observed value of the mean small separation of 70 Oph A in order to obtain an independent determination of the value of the age, the mixing-length parameter and the initial

helium abundance of the 70 Ophiuchi system. This is illustrated in more detail in Fig. 7 where the value of the mean small separations of 70 Oph A for models of 70 Oph AB computed for different initial helium abundances and mixing-length parameters is shown. As expected, the mean small separation is found to significantly decrease with the age. The increase of the age of the system is directly correlated to the decrease of the initial helium abundance, which is in turn directly related to the increase of the value of mixing-length parameter needed to reproduce the observed location of 70 Oph A in the HR diagram and the observed mean large separation. We thus conclude that the observation of the mean small separation of 70 Oph A will lift the degeneracy between the value of the mixing-length parameter and the initial helium abundance by adding a strong observational constraint on the age of the system and will therefore enable an independent and precise determination of the mixing-length parameter and the initial helium abundance of the 70 Ophiuchi system.

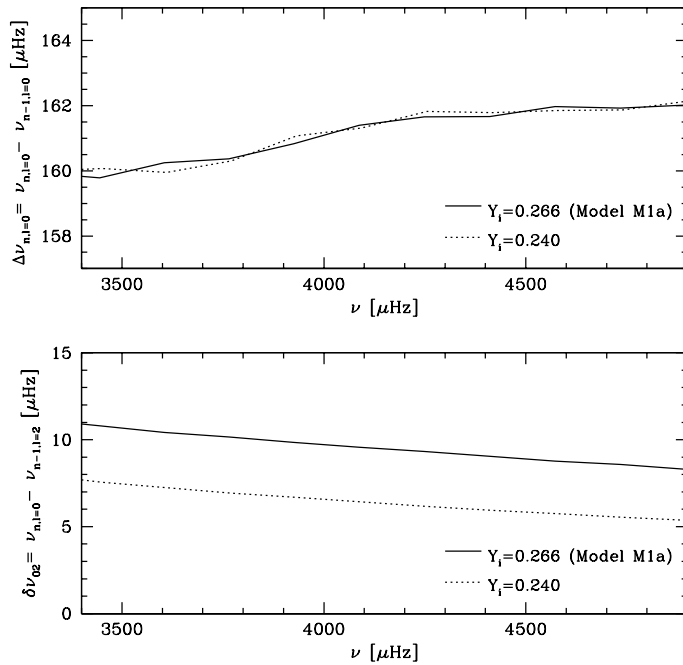


Fig. 6. Large and small separations corresponding to the models of 70 Oph A whose location in the HR diagram is shown in Fig. 5. The solution with $Y_i = 0.266$ has a solar mixing-length parameter, while the model with $Y_i = 0.240$ has been computed with $\alpha = 1.25\alpha_\odot$.

The mean small separation of 70 Oph A has unfortunately not been observed. The mono-site nature of current asteroseismic observations coupled to the low resolution of the time series do not enable such a measurement. As discussed in Sect. 2.4, these observations nevertheless suggest that the value of the mean small separation of 70 Oph A is included in a frequency interval centered around the daily alias of $11.57 \mu\text{Hz}$ introduced by the mono-site observations and delimited by the frequency resolution of the time-series ($2.2 \mu\text{Hz}$). As shown in Fig. 7, this constraint on the small separation rules out models of 70 Oph AB with an age higher than about 7 Gyr, an initial helium abundance Y_i lower than about 0.260 and a mixing-length parameter α larger than about $1.05\alpha_\odot$. We thus conclude that current asteroseismic observations suggest that the age of the 70 Ophiuchi system lies between 2 and 7 Gyr with a mixing-length parameter between about 0.8 and $1.05\alpha_\odot$ and an initial initial helium abun-

dance Y_i between 0.260 and 0.290 when the constraint of a solar mixing-length parameter is relaxed.

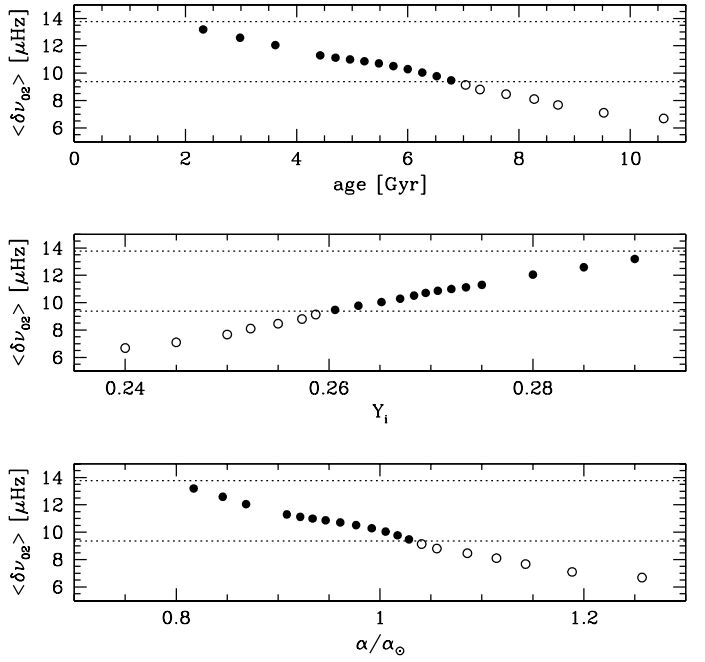


Fig. 7. Mean small separation $\delta\nu_{02}$ of the component A for different models of 70 Ophiuchi. Dots and open symbols correspond to solutions with an age lower and higher than 7 Gyr, respectively. Dotted lines indicate the allowed frequency interval for the mean small separation suggested by current asteroseismic observations.

4.2. Models with the new solar mixture

In order to test the sensitivity of the global parameters determined for 70 Oph AB on the adopted solar mixture, we decided to redo the whole calibration using the solar mixture proposed by Asplund et al. (2005) complemented with the neon abundance of Cunha et al. (2006). This results in a lower solar value of the ratio between the mass fraction of heavy elements and hydrogen $(Z/X)_\odot = 0.0178$. We recall here that solar models evolved with this new abundance mixture give worse agreement with helioseismic constraints (see e.g. Guzik 2006). For these computations, we use OPAL opacity tables calculated with the corresponding solar mixture and the mixing-length parameter is fixed to its solar calibrated value. We then find the following solution: $t = 6.3 \pm 1.0$ Gyr, $M_A = 0.90 \pm 0.02 M_\odot$, $M_B = 0.73 \pm 0.01 M_\odot$, $Y_i = 0.255 \pm 0.018$ and $(Z/X)_i = 0.0220 \pm 0.0023$. The position in the HR diagram of this model of 70 Oph A and B (denoted model M2 in the following) is given in Fig. 3 and its global features are reported in Table 3. We note that this solution calibrated with the new solar abundances presents a different initial chemical composition, but no other significant deviation from the global parameters of the M1 models computed with the solar mixture of Grevesse & Noels (1993). Indeed, the M1 and M2 models share the same age and the same locations in the HR diagram. A lower value of the initial helium abundance is then found for the M2 model in order to compensate for the decrease in the initial ratio between the mass fraction of heavy elements and hydrogen resulting from the lower solar value $(Z/X)_\odot$. As it happens for the Sun and for α Centauri A (see Miglio & Montalbán 2005),

the models of 70 Oph A computed with the solar mixture of Grevesse & Noels (1993) exhibit a deeper convective zone compared with the M2 model, but the uncertainty in the observational constraints do not enable to reveal this difference that can be masked by other choice of parameters.

4.3. Models without atomic diffusion

The effects of atomic diffusion on the calibration of the 70 Ophiuchi system are also studied by computing models without diffusion. For these computations, the solar mixture of Grevesse & Noels (1993) is used and the mixing-length parameter is fixed to its solar calibrated value. Thus the same calibration is made as for the M1 models except for the inclusion of atomic diffusion. We then obtain the solution (hereafter referred as M3) $t = 7.2 \pm 1.2$ Gyr, $M_A = 0.90 \pm 0.02 M_\odot$, $M_B = 0.73 \pm 0.01 M_\odot$, $Y_i = 0.254 \pm 0.018$ and $(Z/X)_i = 0.0266 \pm 0.0025$. The characteristics of this solution are given in Table 3 while the location of both components in the HR diagram is shown in Fig. 3. By comparing model M3 with the M1 models, we see that the initial chemical composition differs. Indeed, the M1 models are characterized by a higher initial ratio between the mass fraction of heavy elements and hydrogen than the M3 solution because of the inclusion of atomic diffusion. Moreover the initial helium abundance of the model without diffusion is lower and this results in an increase of the age of about 1 Gyr.

Figure 8 shows the effects of atomic diffusion on the frequencies of 70 Oph A. The differences between the frequencies of the M2 and the M1b models of 70 Oph A (defined as $\nu_{n0}(M1b) - \nu_{n0}(M3)$) show that the slightly lower value of the surface abundance in helium of the model computed without atomic diffusion (difference of about 4 %) does not significantly change the value of the frequencies. For a low-mass star like 70 Oph A, the effects of atomic diffusion are indeed small because of the large mass contained in its convective zone. We thus conclude that the change in the frequencies introduced by the different value of the surface helium abundance that implies a different opacity and, therefore, a different location of the boundary of the convective zone is too small to be clearly revealed.

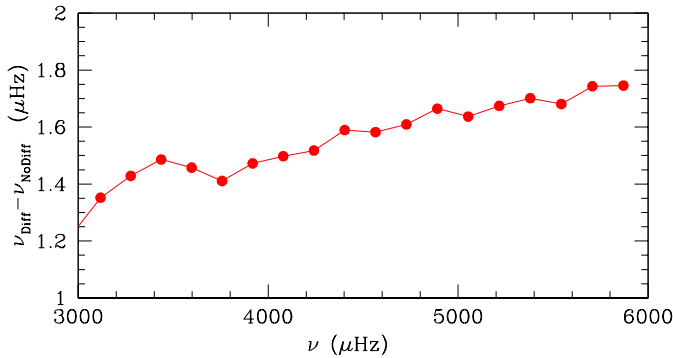


Fig. 8. Differences of frequencies between the model of 70 Oph A computed with the inclusion of atomic diffusion (solution M1b) and the model of 70 Oph A computed without atomic diffusion (solution M3).

5. Conclusion

Our calibration of the 70 Ophiuchi AB shows that a solution correctly reproducing all asteroseismic and non-asteroseismic observational constraints now available for both stars can be determined. An age of 6.2 ± 1.0 Gyr is found with an initial helium mass fraction $Y_i = 0.266 \pm 0.015$ and an initial metallicity $(Z/X)_i = 0.0300 \pm 0.0025$ when atomic diffusion is included and a solar value of the mixing-length parameter is assumed. Concerning the mixing-length parameter, we found that current asteroseismic measurements do not allow a firm independent determination of this value that will only be possible with a precise measurement of the mean small separation. The effects of atomic diffusion and of the choice of the adopted solar mixture on the results of the calibration were also studied. We then found that a change of the solar mixture results of course in a different initial chemical composition but does not change significantly the other global parameters. Models computed without atomic diffusion also have a different initial chemical composition than models including diffusion but they also exhibit a slightly higher age (difference of about 1 Gyr).

We finally mention that we took the opportunity of the calibration of the 70 Ophiuchi system to compare and test the theoretical tools used for the modeling of stars for which p-modes frequencies are detected. Thus, the same analysis was performed with three different stellar evolution codes including a coherent input physics: the Geneva code, the CLES code and the CESAM code. Two different calibration methods were also used: the computation of a dense grid of stellar models and a minimization algorithm. We found that the different evolution codes and calibration methods lead to perfectly similar and coherent solutions. This result is comforting in the perspective of the theoretical interpretation of asteroseismic data that are expected from the CoRoT and the Kepler space missions and from future ground-based campaigns.

Acknowledgements. We thank J. Christensen-Dalsgaard for providing us with the Aarhus adiabatic pulsation code. This work has made use of the ORBIT code developed by T. Forveille. A.M. acknowledges financial support from the Prodex-ESA Contract Prodex 8 COROT (C90199). Part of this work was supported by the Swiss National Science Foundation.

References

- Alexander, D. R. & Ferguson, J. W. 1994, *ApJ*, 437, 879
- Angulo, C., Arnould, M., Rayet, M., et al. 1999, *Nuclear Physics A*, 656, 3
- Asplund, M., Grevesse, N., Sauval, A. J., Allende Prieto, C., & Blomme, R. 2005, *A&A*, 431, 693
- Batten, A. H. & Fletcher, J. M. 1991, *PASP*, 103, 546
- Batten, A. H., Fletcher, J. M., & Campbell, B. 1984, *PASP*, 96, 903
- Bazot, M., Bouchy, F., Kjeldsen, H., et al. 2007, *A&A*, 470, 295
- Bedding, T. R. & Kjeldsen, H. 2007, *ArXiv e-prints*, 705
- Bedding, T. R., Kjeldsen, H., Butler, R. P., et al. 2004, *ApJ*, 614, 380
- Bouchy, F. & Carrier, F. 2002, *A&A*, 390, 205
- Burnet, M. & Rufener, F. 1979, *A&A*, 74, 54
- Carrier, F. & Bourban, G. 2003, *A&A*, 406, L23
- Carrier, F. & Eggenberger, P. 2006, *A&A*, 450, 695
- Casagrande, L., Flynn, C., Portinari, L., Girardi, L., & Jimenez, R. 2007, *ArXiv Astrophysics e-prints*
- Casagrande, L., Portinari, L., & Flynn, C. 2006, *MNRAS*, 373, 13
- Caughlan, G. R. & Fowler, W. A. 1988, *Atomic Data and Nuclear Data Tables*, 40, 283
- Cherix, M., Carrier, F., Burki, G., & Blecha, A. 2006, *Memorie della Societa Astronomica Italiana*, 77, 328
- Christensen-Dalsgaard, J. 1997, <http://astro.phys.au.dk/~jcd/adipack.n>
- Cunha, K., Hubeny, I., & Lanz, T. 2006, *ApJ*, 647, L143
- Däppen, W., Mihalas, D., Hummer, D. G., & Mihalas, B. W. 1988, *ApJ*, 332, 261
- Eggenberger, P. & Carrier, F. 2006, *A&A*, 449, 293
- Eggenberger, P., Carrier, F., & Bouchy, F. 2005, *New Astronomy*, 10, 195

- Eggenberger, P., Carrier, F., Bouchy, F., & Blecha, A. 2004a, *A&A*, 422, 247
Eggenberger, P., Charbonnel, C., Talon, S., et al. 2004b, *A&A*, 417, 235
Eggenberger, P., Meynet, G., Maeder, A., et al. 2007, *Ap&SS*, 263
Eggleton, P. P., Faulkner, J., & Flannery, B. P. 1973, *A&A*, 23, 325
Fernandes, J., Lebreton, Y., Baglin, A., & Morel, P. 1998, *A&A*, 338, 455
Flower, P. J. 1996, *ApJ*, 469, 355
Forveille, T., Beuzit, J.-L., Delfosse, X., et al. 1999, *A&A*, 351, 619
Golay, M. 1980, *Vistas in Astronomy*, 24, 141
Grevesse, N. & Noels, A. 1993, in *Origin and evolution of the elements: proceedings of a symposium in honour of H. Reeves, held in Paris, June 22-25, 1992*. Edited by N. Prantzos, E. Vangioni-Flam and M. Casse. Published by Cambridge University Press, Cambridge, England, 1993, p.14, ed. N. Prantzos, E. Vangioni-Flam, & M. Casse, 14
Guzik, J. A. 2006, in *ESA Special Publication, Vol. 624, Proceedings of SOHO 18/GONG 2006/HELAS I, Beyond the spherical Sun*
Hummer, D. G. & Mihalas, D. 1988, *ApJ*, 331, 794
Iglesias, C. A. & Rogers, F. J. 1996, *ApJ*, 464, 943
Kjeldsen, H., Bedding, T. R., Butler, R. P., et al. 2005, *ApJ*, 635, 1281
Kurucz, R. L. 1998, <http://kurucz.harvard.edu/grids.html>
Lejeune, T., Cuisinier, F., & Buser, R. 1998, *A&AS*, 130, 65
Luck, R. E. & Heiter, U. 2005, *AJ*, 129, 1063
Martić, M., Lebrun, J.-C., Appourchaux, T., & Korzennik, S. G. 2004, *A&A*, 418, 295
Meynet, G. & Maeder, A. 2000, *A&A*, 361, 101
Miglio, A. & Montalbán, J. 2005, *A&A*, 441, 615
Mihalas, D., Däppen, W., & Hummer, D. G. 1988, *ApJ*, 331, 815
Monteiro, M. J. P. F. G., Lebreton, Y., Montalban, J., et al. 2006, in "The CoRoT Mission", (Eds) M. Fridlund, A. Baglin, J. Lochard, L. Conroy, ESA Publications Division, *ESA Spec.Publ. 1306 (2006)* 363, 363
Morel, P. 1997, *A&AS*, 124, 597
Mosser, B., Bouchy, F., & Martić, M. 2007, *ArXiv e-prints*, 712
Pourbaix, D. 2000, *A&AS*, 145, 215
Pourbaix, D., Tokovinin, A. A., Batten, A. H., et al. 2004, *A&A*, 424, 727
Ramírez, I. & Meléndez, J. 2005, *ApJ*, 626, 465
Rogers, F. J. & Nayfonov, A. 2002, *ApJ*, 576, 1064
Santos, N. C., Israelian, G., & Mayor, M. 2004, *A&A*, 415, 1153
Scuflaire, R., Montalbán, J., Théado, S., et al. 2007a, *Ap&SS*, in press
Scuflaire, R., Théado, S., Montalbán, J., et al. 2007b, *Ap&SS*, in press
Söderhjelm, S. 1999, *A&A*, 341, 121
Turcotte, S., Richer, J., Michaud, G., Iglesias, C. A., & Rogers, F. J. 1998, *ApJ*, 504, 539